

## Experimental and Numerical Investigations of Composite Concrete–Steel Plate Shear Walls Subjected to Axial Load

Jinan Laftah Abbas <sup>a,b\*</sup>, Abbas AbdulMajeed Allawi <sup>c</sup>

<sup>a</sup> Ph.D. Student, Civil Engineering Department, University of Baghdad, Baghdad, Iraq.

<sup>b</sup> Lecturer, Civil Engineering Department, University of Diyala, Diyala, Iraq.

<sup>c</sup> Professor, Civil Engineering Department, University of Baghdad, Baghdad, Iraq.

Received 23 July 2019; Accepted 31 October 2019

### Abstract

This research is presented experimental and numerical investigations of composite concrete-steel plate shear walls under axial loads to predicate the effect of both concrete compressive strength and aspect ratio of the wall on the axial capacity, lateral displacement and axial shortening of the walls. The experimental program includes casting and testing two groups of walls with various aspect ratios. The first group with aspect ratio  $H/L=1.667$  and the second group with aspect ratio  $H/L=2$ . Each group consists of three composite concrete -steel plate wall with three targets of cube compressive strength of values 39, 54.75 and 63.3 MPa. The tests result obtained that the increase in concrete compressive strength results in increasing the ultimate axial load capacity of the wall. Thus, the failure load, the corresponding lateral displacement and the axial shortening increased by increasing the compressive strength and the rate of increase in failure load of the tested walls was about (34.5% , 23.1%) as compressive strength increased from 39 to 63.3 MPa for case of composite wall with aspect ratio  $H/L=1.667$  and  $H/L=2$ , respectively. The effect of increasing aspect ratio on the axial load capacity, lateral displacement and axial shortening of the walls was also studied in this study. Compared the main performance characteristic of the testing walls, it can be indicated that the walls with aspect ratio equal to (2) failed under lower axial loads as compared with walls with aspect ratio equal to 1.667 ratios by about (5.8, 12, 15.6 %) at compressive strength (39, 54.75, 63.3 MPa), respectively and experienced large flexural deformations. The mode of failure of all walls was characterized by buckling of steel plates as well as cracking and crushing of concrete in the most compressive zone. Nonlinear three-dimensional finite element analysis is also used to evaluate the performance of the composite wall, by using ABAQUS computer Program (version 6.13). Finite element results were compared with experimental results. The comparison shows good accuracy.

**Keywords:** Composite Concrete-Steel Plate Shear Walls; Axial Load; Compressive Strength; Aspect Ratio; Lateral Displacement; Shortening; Failure Mode.

### 1. Introduction

Concrete filled steel tubes have been widely used in bridges and high- rise buildings for its advantages of high-load bearing capacity, good seismic behavior and fast construction [1, 2]. Recently, a new kind of composite wall structure with a steel plate in addition to concrete, chiefly employed in super -high rise building, missile as well as plate resistance walls for the great bearing capacity that it has and reducing in its thickness. The axial compression loading is considered as a critical case because of the relative motion happens between the faceplate and infill concrete. On the other hand,

\* Corresponding author: [jinanlaftah19@gmail.com](mailto:jinanlaftah19@gmail.com)

 <http://dx.doi.org/10.28991/cej-2019-03091420>



© 2019 by the authors. Licensee C.E.J, Tehran, Iran. This article is an open access article distributed under the terms and conditions of the Creative Commons Attribution (CC-BY) license (<http://creativecommons.org/licenses/by/4.0/>).

the local instability of the steel plate might cause weak cooperative action, which has a large effect on the axial performance of composite walls. Lately, some of associated studies on the axial performance of composite walls with embedded connectors have been carried out. Othuman Mydin (2011) investigated the effect of buckling of steel plate on the axial compressive bearing capacity of lightweight steel-foamed concrete-steel composite walls under axial compression test of 12 specimens were carried out [3]. Xiaowei et al. (2013) studied the response of double- steel plate concrete walls. The effects of the axial force and thickness of the faceplate were studied.

They showed a numerical study on the composite walls under axial compressive and cyclic loadings. The proposed model succeeded in predicts of shear strength of the walls but underestimated the displacement of peak [4]. Steel-concrete-steel (SCS) sandwich structures containing two steel faceplates infilled with lightweight cement composite material has been indicated by Liew et al. (2017). The recent innovations of SCS sandwich structures applied to blast, fatigue, impact, as well as static loads were assessment. The test explanations displayed that SCS sandwich walls demonstrated admirable compression resistance and post-peak ductility in the case of providing J-hook connectors to avoid face plates separation [5]. Elmatzoglou and Avdelas (2017) evolved a dependable three-dimensional finite element model for nonlinear analysis of double- steel composite walls, which can efficiently investigate the response of the composite wall in terms of accuracy and saving time focusing on the shear connection [6]. The local buckling behavior of steel plates in concrete-filled double steel plate composite shear walls under axial compression has been investigated using the ABAQUS computer program. The results showed that local buckling of the steel plates constantly happens between the neighboring rebar for the rebar layout of the same spacing in two orthotropic directions. Subsequently, the steel plates buckle, the rebar neighboring to the buckling location resists excessive tensile forces, as well as the tensile forces rises with the reduction of the rebar spacing [7]. Validation studies have been undertaken using the experimental results of four axial compression tests reported by Akiyama et al. (1991) and Usami et al. (1995), Choi et al. (2014) and Zhang (2014) [8-11].

The proposed model has been proved to be effective in terms of predicted yield, ultimate load, displacement, and final failure mode displacement and final failure mode, and it is suitable for further numerical studies on shear connection behavior at the steel-concrete interface due to its accuracy and simplicity. Hao et al. (2017) investigate the axial compression performance of a composite shear wall, having various layout arrangements of steel plate. This study consisted of three experiments. Two experiments with built-in steel plate, and the other one with two skins of steel plate. The gross dimensions of all tested walls were the same. The experimental results showed that the diverse layout arrangements of steel plate have an excessive effect on its buckling that can influence the bearing capacity of the plate. Axial compression of 15 specimens of double –skin steel-concrete shear wall with “J” interlocking was carried out and put forward by Huang and Liew (2016) by considering the buckling influenced of the steel plate, the calculation formula of axial compressive bearing capacity was put forward [13]. Qin et al. (2017) suggested a methodology to calculate the steel plate strength with the restriction of both concrete and shear studs depending on the explicit solution for local buckling of steel plate in composite shear walls exposed to uniform axial compression with elastically rotational restraint at loaded as well as unloaded edges [14]. Eslami and Rahai (2018) carried out experimental investigations on the behavior of fiber-reinforced lightweight concrete-filled double steel plate shear wall [15]. Anwar and Najam (2018) consider some key subjects associated with the application and design of composite structural components to result in good execution of high-rise buildings versus gravity as well as lateral loads. A unified approach to accomplish the axial-flexural capacity of several composites and complex cross-sections are offered. The analysis of all composite cross-sections can be achieved as well as essential considerations for an operative design of composite members (floors, columns, shear walls, link beams, and transfer systems) is existing. In addition, the practical aspects of composite concrete-steel structure in tall buildings are also presented [16]. According to this review, it is clear that there is a need to study the behavior of composite concrete-steel plate shear wall with embedded connectors. In this study, strengthening of the concrete walls by using external steel faceplates have an important effect on raising the bearing capacity of the walls and decreasing the lateral and axial displacement in comparison with the concrete walls, by varying some parameters such compressive strength, as well as an aspect ratio of the wall.

## 2. Experimental Work

The plan of experimental work includes casting and testing six of composite walls divided into two groups, each group contains three composite walls, with the various value of concrete compressive strength. The first one with normal cube compressive strength (39 MPa), the second with high cube compressive strength (54.75 MPa) and the third with high compressive strength (63.3 MPa). These specimens were divided into three groups depending on the type of loading. Figure 1 shows the experimental program used throughout this work. The composite walls for each group with dimensions of total length (600 mm), a thickness of (55mm), same thickness of steel plates ( $t_p=2$  mm), same slenderness ratio ( $S/t_p=75$ ) where  $S$  represents the distance between steel channels equal to (150mm), but with different aspect ratio of wall. The first group with an aspect ratio ( $H/L=1.667$ ), while the second group with an aspect ratio ( $H/L=2$ ). The details of all groups can be shown in Figure 2 and Table1. In all groups, the tested walls consisted of a test – wall part and a base. The base of the wall was used for fixing the laboratory rigid floor and act as a means to fix the steel plate

which embedded into the wall base through the cage reinforcement. The wall base was (350mm) thick, (400mm) width, and (600 mm) length and reinforced by using  $\phi 12$  mm deformed steel bar as longitudinal reinforcement (4  $\phi 12$  top and 4  $\phi 12$  Bottom reinforcement) and using of  $\phi 10$  mm deformed steel @ 125mm as stirrups shear reinforcement.

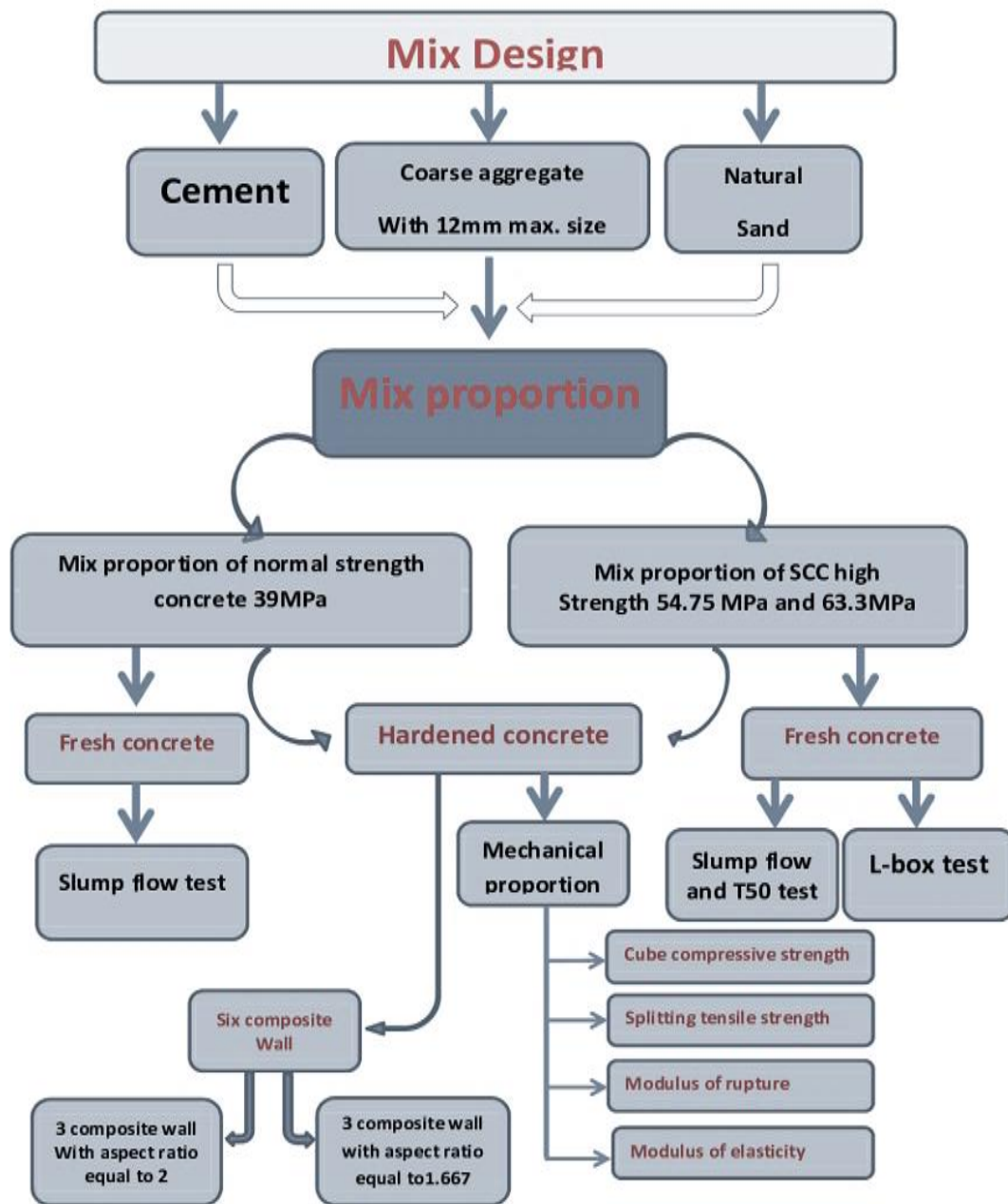


Figure 1. Schematic representation of experimental program

Table 1. Details of the two group

Group	Wall dimensions	Cube Compressive strength	Thickness of plate tp(mm)	Steel plate Slenderness ratio (s/tp)	Aspect ratio H/L	Rein. Ratio
1	1000×600×55	39	2	75	1.667	7.27%
		54.75				
2	1200×600×55	63.3	2	75	2	7.27%
		39				
		54.75				
		63.3				

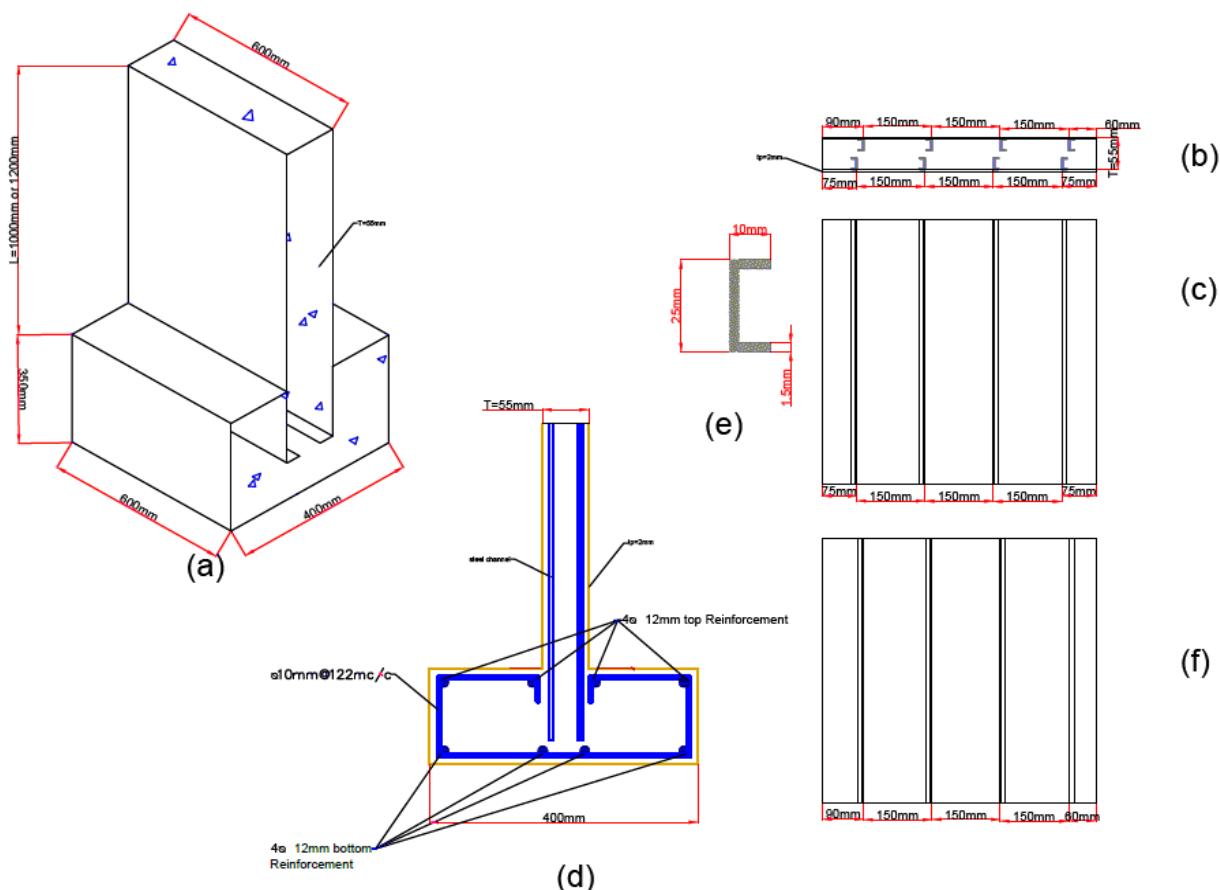


Figure 2. Details of all groups (a) Isometric view of the wall; (b) Top of wall; (c) Right plate with steel channel; (d) Section through all wall; (e) Dimension of steel channel; (f) Left plate with steel channel

2.1. Materials

The materials used in concrete mixes are Ordinary Portland cement (Type I), natural sand which has a specific gravity of 2.6 and sulfate content SO<sub>3</sub>% (0.11%) by sand weight and crushed gravel with a maximum size of particles of (12mm). The bulk specific gravity of this aggregate is 2.8 and sulfate content 0.08 %. The grading of both the coarse and fine aggregate can be shown in Figure (3), Tables 2 and 3.

Table 2. Grading of coarse aggregate

Sieve size (mm)	%Passing	Limit of the Iraqi specifications. (No. 45 / 1984)
20	100	100
14	100	90-100
10	72	50-85
4.75	0.98	0-10
Pan	Zero	Zero

Table 3. Grading of fine aggregate

Sieve size	%Passing	Limit of the Iraqi specifications. (No. 45 / 1984)zone two
10	100	100
4.75	91	90-100
2.36	78.4	75-100
1.18	62	55-90
0.6	47	35-59
0.3	19	8-30
0.15	4	0-10
Pan	Zero	Zero

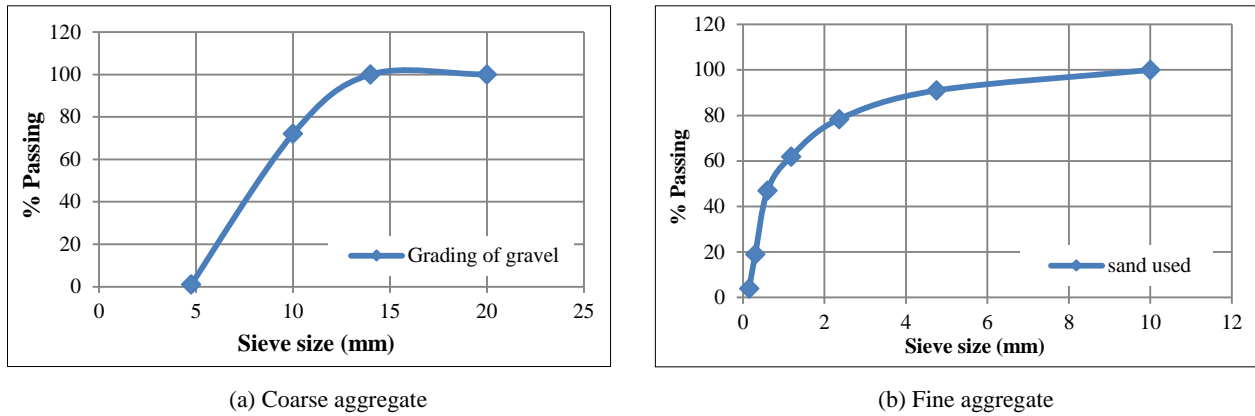


Figure 3. Grading of materials

Two types of mix were made in the present work. Firstly is normal strength concrete mix which was designed according to (ACI, 2014) [17]. The fresh properties of concrete with strength target 39MPa were obtained from the slump flow test, and slump was measured (180 mm). Secondly is high strength self-compacted concrete mix SCC). For the production of SCC mix, Superplasticizer which is commercially known as (Sika viscocrete, 5930), as well as silica Fume is used. Superplasticizer concrete showing a large increase in slump without segregation. Thus, adding of Superplasticizer which meets with (ASTM C 494 / C 494 M-99) [18] types G and F result in improvement in the workability of the concrete mix which was designed according to (EFNARC, 2002) [19]. The weight of materials for normal strength concrete mix and (SCC) mix used in the present work can be shown in Table 4 and Table 5. Both of slump flow, T50, and L-box tests have been used in present work in order to study the fresh properties of self-compacting concrete as shown in Figure 4, Figure 5 and Table 6. The slump flow test is used to assess the horizontal free flow of SCC in the absence of obstructions. The test method is based on the test method for determining the slump. The diameter of the concrete circle is a measure for the filling ability of the concrete. In addition, the L-box test is a widely used test that assesses filling and passing ability of SCC, and a serious lack of stability (segregation) can be detected visually. Segregation may also be detected by subsequently sawing and inspecting sections of the concrete in the horizontal section. The testing apparatus consists of rectangular section box of L shape with horizontal and vertical part that separated by using a moveable gate, in front of which vertical lengths of reinforcement bar are fitted. This test is satisfied by measuring the distance H1 and H2, in addition, to calculate the blocking ratio (H2/H1) when the concrete flowing is stopped. The whole test should be finished in five minutes.

Table 4. Mix proportions of normal strength concrete

Mix no.	w/c	Water (kg/m <sup>3</sup> )	Cement content (kg/m <sup>3</sup> )	Sand content (kg/m <sup>3</sup> )	Gravel content (kg/m <sup>3</sup> )	S.P (L/m <sup>3</sup> )	Silica Fume (kg/m <sup>3</sup> )	Cube compressive Strength f <sub>c</sub> (MPa (28 days))
1	0.55	203	370	750	792	-	-	38.63

Table 5. Mix proportions high strength self-compacted concrete

Mix No.	Type of test	Result	EFNARC requirements	Limits of ACI-237	
1	Slump	D(mm)	725	650-800	450-760
	T50 tests	(sec)	2.5	2-5	2-5
	L-box test	(H2/H1)	1	0.8-1	0.8-1
2	Slump	D(mm)	715	650-800	450-760
	T50 tests	(sec)	3	2-5	2-5
	L-box test	(H2/H1)	1	0.8-1	0.8-1

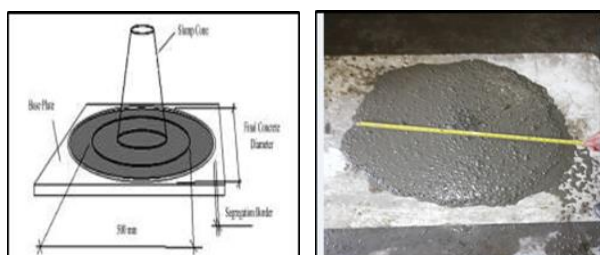


Figure 4. Slump flow test measurements test for SCC material

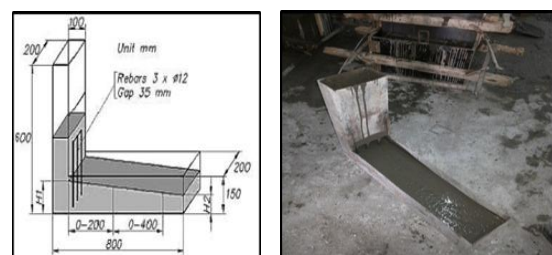


Figure 5. L-box test for

**Table 6. Test results of fresh SCC**

Mix no.	w/c	Water (kg/m <sup>3</sup> )	Cement content (kg/m <sup>3</sup> )	Sand content (kg/m <sup>3</sup> )	Gravel content (kg/m <sup>3</sup> )	S.P (L/m <sup>3</sup> )	Silica Fume (kg/m <sup>3</sup> )	Cube compressive Strength $f'_c$ MPa (28 days)
1	0.46	185	400	798	760	5.5	20	52
2	0.36	160	440	770	880	13.5	22	61.4

The mechanical properties for both rebar and steel plates used were obtained from the tensile testing of three samples according to ASTM designation (C370 – 05a, 2005) [20]. Tables 7, 8 and 9 give the yield and ultimate stress of the tested rebar, steel plates, as well as steel channel respectively.

**Table 7. Mechanical properties of steel bars reinforcement**

Nominal diameter	Surface texture	Yield stress (MPa)	Ultimate stress (MPa)	<b>ES</b> (GPa)	Elongation%
12	deformed	550	640	200	10.5
10	deformed	565	655	200	8.5

**Table 8. Mechanical properties of steel plates**

Thickness	Surface texture	Yield stress (MPa)	Ultimate stress (MPa)	<b>ES</b> (GPa)	Elongation%
2	mild steel	290	370	203	32.6

**Table 9. Mechanical properties of steel channels**

Thickness (mm)	Surface texture	Yield stress (MPa)	Ultimate stress (MPa)	<b>ES</b> (GPa)	Elongation%
1.5	mild steel	275	355	193	34.2

Through the casting of the walls, three 150×150×150 mm cubes were cast and used to measure the compressive strength ( $f'_c$ ), three cylinders of 150×300 mm used for measuring split tensile strength ( $f_{ct}$ ). In addition, three 500×100×100 mm prisms were cast and used to obtain the modulus of rupture for concrete ( $f_r$ ) for each group. The hardened properties of the tested wall can be shown in Table 10. Then after that, the walls were cast. After finishing the casting of walls. They were demolded 24 hours, and then after that, the mold and the wooden beams removed, after that the walls cured by using dump blanket (cover) and scattered continuously with water for 28 days. After the end of the curing period, the walls were white-painted to assistance in the observation of crack and improvement through testing as shown in Figure 6.

**Table 10. Hardened properties of the tested walls**

Compressive strength $f'_c$ (MPa) on the day of the test	$f_{ct}$ (MPa), on the day of the test (cylinders)	$f_r$ (MPa), on the day of the test (prisms)	Modulus of elasticity <b>Ec*</b> (MPa)
39	3.4	6.09	26253
54.75	4.15	6.45	31105
63.3	4.43	6.87	33446

\*The values of Ec were derived from  $(4700\sqrt{f'_c})$  provided by (ACI 318M-2014)



**Figure 6. Casting of the walls**

**2.2. Test Set-Up**

All composite walls are tested by using the hydraulically universal testing machine of (3000 kN) capacity available in Al-Mustansiriyah University. The tested walls were axially loaded by making some arrangements before the test. The composite walls were equipped for testing by setting the positions of them over steel plate of dimension (2×44×70 cm) (thickness×width×length). Series of dial gauges- which are used for monitoring the response of the tested wall- were fixed in their position. Besides, a steel I-section fixed tightly to the test machine by many clamps at the top. A steel frame consisted of a steel channel (C55 mm or C70 mm) welded very well to the flange of I-steel section of dimension (72 cm) and web height (23 cm) and is strengthened by using stiffener and this operation made very carefully as well as with high accuracy in order to ensure satisfying straight lines and no gap allowed to form within support. After the top hinge support has been fixed, leveling the wall panel to satisfy the perpendicularity of the wall panel and applying the load to the failure of wall. The composite walls were subjected to monotonic-static loads in successive increments, until failure. See Figure 7.



Figure 7. Universal testing machine used to test the walls

**3. Failure Modes**

The failure mode of all the composite walls was initiated by local buckling of the steel side plates as well as cracking and crushing of concrete. The local buckling of steel plate gradually increased with the increase in the load step till its maximum thickness reached failure load. Local buckling of steel plates happens previous than the yield of the steel plate that bends slightly after buckling because of uniform compression, and the deflection in the central section at top height of the walls is more than the lateral displacement at the two edges, as well as the flexural shortening in the central section is greater than the shortening at the two edges. In addition, a brittle failure such as concrete cracking and crushing of concrete which were the dominant damage pattern of concrete are also shown. Concrete cracks were accumulated at the base of the wall beside other cracks which separate in the front and the back height of concrete as well as crushing of the concrete infill in the top region of the composite wall. The concrete infill had the ability to prevent the composite wall from local buckling. Concrete crushing of the concrete infill occurs in the top region of the composite wall. The concrete infill had the ability to prevent the composite wall from local buckling. From observation, it can be shown that there was no separation of the steel plate from the concrete core until near failure, indicating that the steel channel was able to hold the steel sheeting and the infill together to enable them to resist the applied load in composite action. The failure mode of the two groups can be shown in Figures 8 and 9.



(a) Right side

(a) Left side

(a) Right side

(b) Left side

Normal strength concrete  $f'c = 39\text{MPa}$

High strength concrete  $f'c = 54.75\text{MPa}$



(a) Right side (b) Left side

High strength concrete  $f_c = 63.3 \text{ MPa}$

Figure 8. Failure mode of the tested wall (group 1)



(a) Right side

Normal strength concrete  $f_c = 39 \text{ MPa}$



(a) Left side



(a) Right side

High strength concrete  $f_c = 54.75 \text{ MPa}$



(a) Left side



(a) Right side

High strength concrete  $f_c = 63.3 \text{ MPa}$



(a) Left side

Figure 9. Failure mode of the tested walls (group2)

## 4. Experimental Results

The general behavior of all the composite walls is studied while varying some parameters, such as concrete strength and aspect ratio of the wall.

### 4.1. Effect of Concrete Strength

The increase in compressive strength of concrete enhances the ultimate axial load capacity of the wall and it should have an effect on the crushing strength of the wall which can affect the failure loads of the walls. Thus, the increase in concrete strength could affect the initiation of the main diagonal crack. All walls in each group have the same thickness as the plate, the same thickness of the wall, the same slenderness and reinforcement ratios with a different value of compressive strength. See Table 1. In these figures, the lateral displacement at the top and mid-height of the walls, as well as the axial shortening of the walls, decreases as the compressive strength increased at the same load. Besides, the failure load increased with an increase in compressive strength.



Three targets of cube compressive strength values of 39, 54.75 and 63.3 MPa, were supplied for each group in this study to evaluate their effect on the axial capacity of the walls with the same thickness. Besides, for the case of composite wall with aspect ratio 1.667 (group1), increasing the compressive strength from (39 MPa) to high strength (54.75 MPa) results in increasing in failure load, the corresponding lateral displacement at top and mid-height of the wall as well as the axial shortening by about (18.2, 12, 5.3, 15.8%), respectively and by about (13.8, 12.3, 20, 8.2%), respectively as concrete strength increased from 54.75 to 63.3 MPa. See Figure 10.

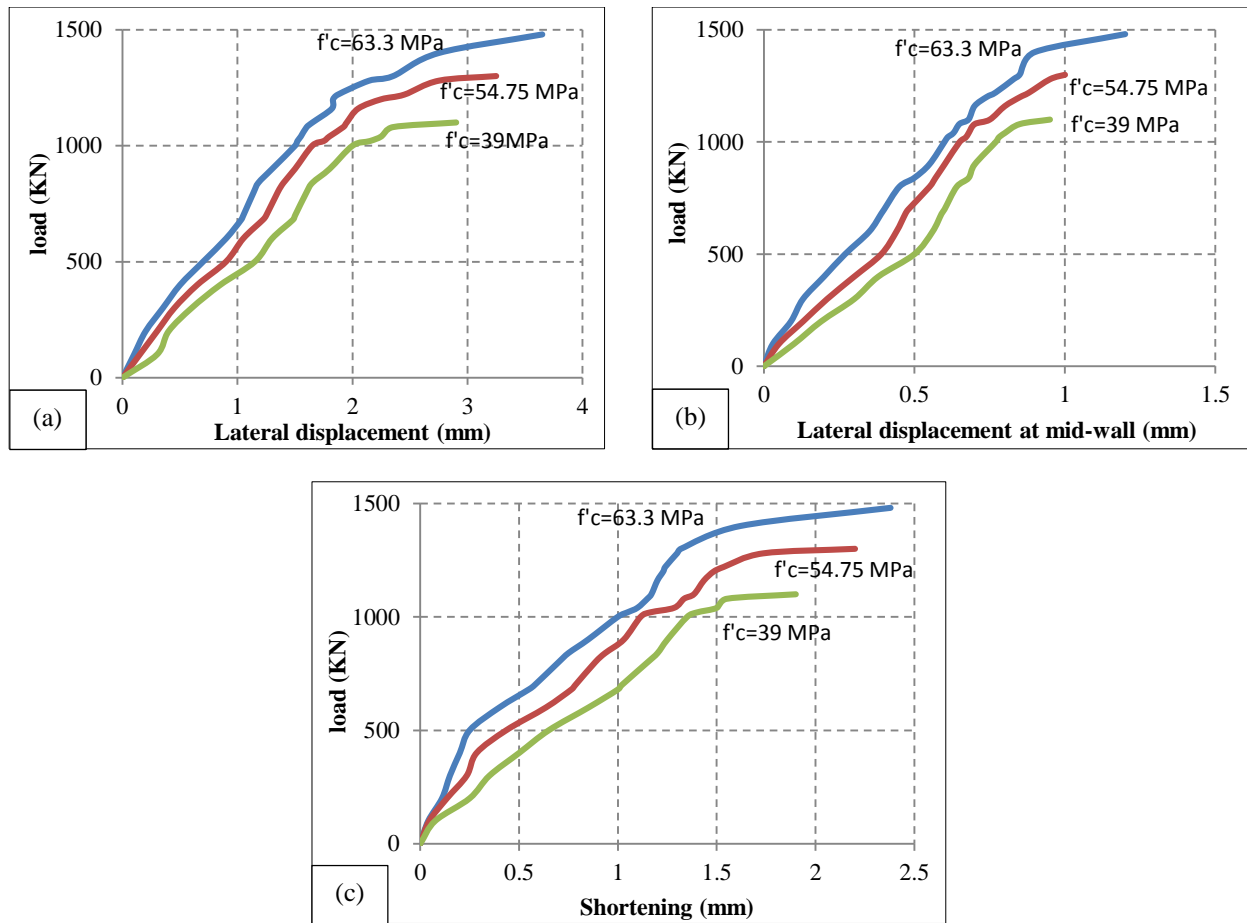
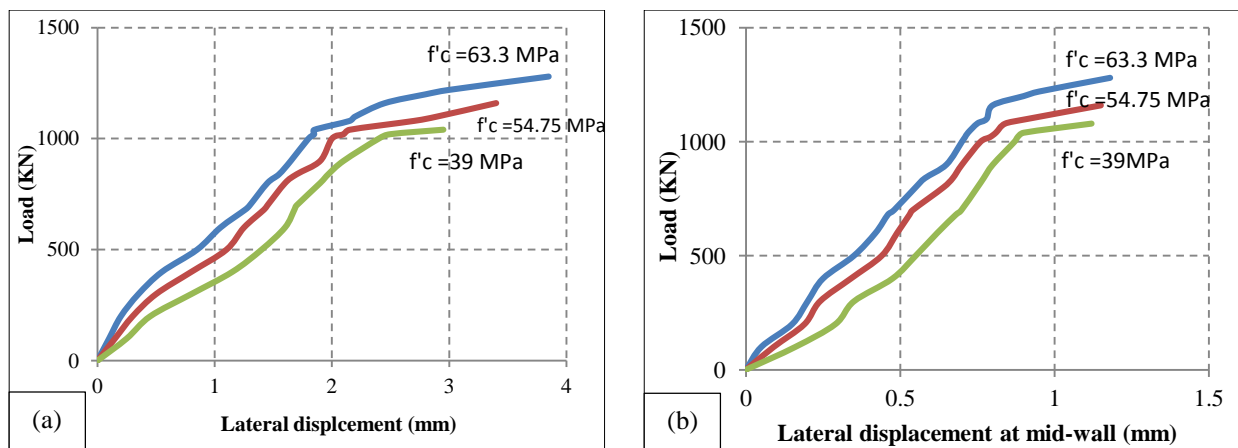


Figure 10. Results of the first group (a) Load versus lateral displacement at the top height of the wall; (b) Load versus lateral displacement at mid-wall; (c) Load versus axial shortening

According to Figure 11, it can be indicated that increasing compressive strength from (39 MPa) to high strength (54.75 MPa) led to an increase in failure load, the corresponding lateral displacement at top and mid-height of the wall, as well as the axial shortening by about (11.5, 15.2, 2.7, 9%), respectively and by about (10.3, 13.2, 2.7, 10.4%), respectively as concrete strength increased from 54.75 to 63.3 MPa.



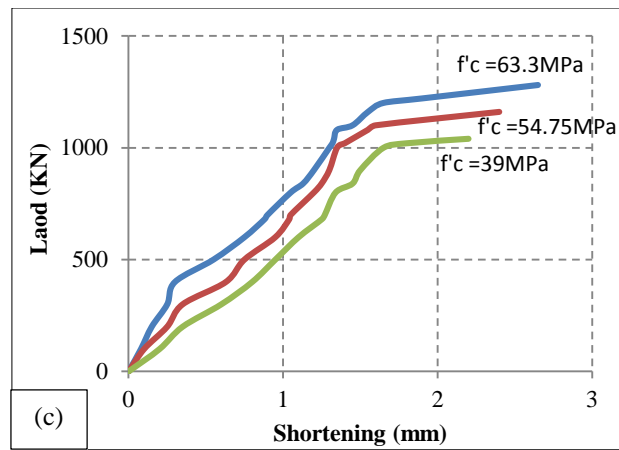


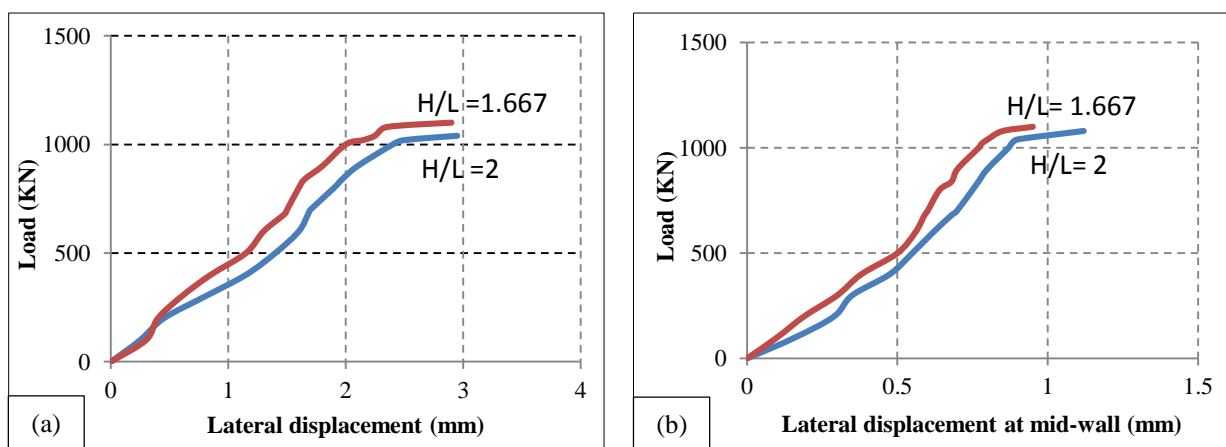
Figure 11. Results the second group (a) Load versus lateral displacement at the top height of the wall; (b) Load versus lateral displacement at mid-wall; (c) Load versus axial shortening

4.2. Effect of Aspect Ratio

The aspect ratio is regarded as an important parameter that affects the behavior of the composite walls. The ultimate load is highly affected by increasing the aspect ratio as shown in the below figures which show the influence of aspect ratio on failure load values.

Compared to the main performance characteristic of the testing walls, it can be shown that the walls with aspect ratio equal to 2 failed under lower axial loads as compared with walls with aspect ratio equal to 1.667. These walls experienced large flexural deformations. The mode of failure was characterized by buckling of steel plates and extensive flexural cracking and concrete crushing in the most compressive zone. Besides, walls with an aspect ratio equal to (1.667) have larger bearing capacity at initial cracking, yield point, and maximum strength than those for walls with higher aspect ratio. A comparison was made between two walls with different aspect ratio 1.667 and 2. It can be noticed from this comparison that increasing aspect ratio led to decreasing the failure load and increasing the corresponding lateral displacement at the top and mid-height of the wall as well as the axial shortening at failure load. Moreover, the lateral displacement and shortening for a composite wall with higher aspect ratio are less than that for the composite wall with a low aspect ratio at the same load.

Figures 12 to 14 show the effect of aspect ratio on the values of lateral deflection at top and mid-height as well as shortening of walls versus axial load. In these figures, a comparison between two walls of the same slenderness and reinforcement ratio was made but with different aspect ratio. As concerned with Figure 12, a comparison between two composite walls was made. The two walls had the same compressive strength (39 MPa) but with different aspect ratios. Increasing aspect ratio led to decreasing the failure load and increasing the corresponding lateral displacement at the top and mid-height of the wall as well as the axial shortening at failure load by about (5.8, 1.7, 17.9, 15.8%).



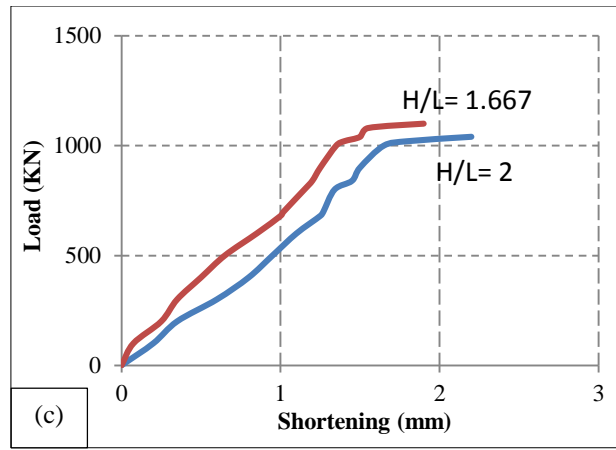


Figure 12. Axial load- lateral displacement at compressive strength equal to 39 MPa (a) At the top height of the wall; (b) At the mid-height of the wall

For the case of composite wall with compressive strength 54.75 MPa, increasing aspect ratio from 1.667 to 2 led to the decreasing the failure load and increasing the corresponding lateral displacement at top and mid-height of the wall as well as the axial shortening at failure load by about (12, 4.6, 15, 9%), respectively. See Figure 13.

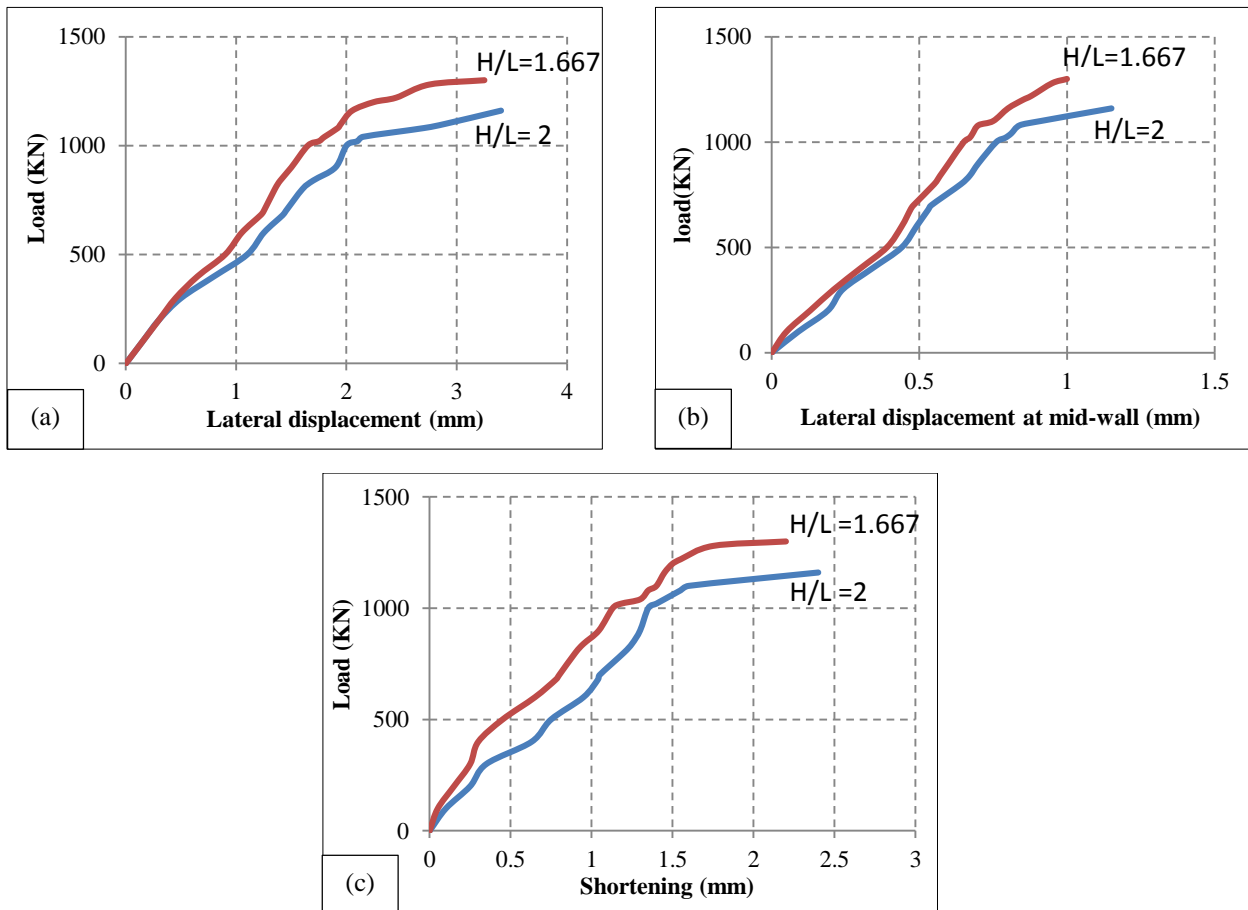


Figure 13. Axial load- lateral displacement at compressive strength equal to 54.75 MPa (a) At the top height of the wall; (b) At mid-height of the wall (continued)

Besides, at compressive strength 63.3 MPa ,increasing aspect ratio from 1.667 to 2 results in decreasing the failure load and increasing the corresponding lateral displacement at top and mid-height of the wall as well as the axial shortening at failure load by about (15.6, 5.5, 1.7, 11.3%), respectively as shown in Figure 14.

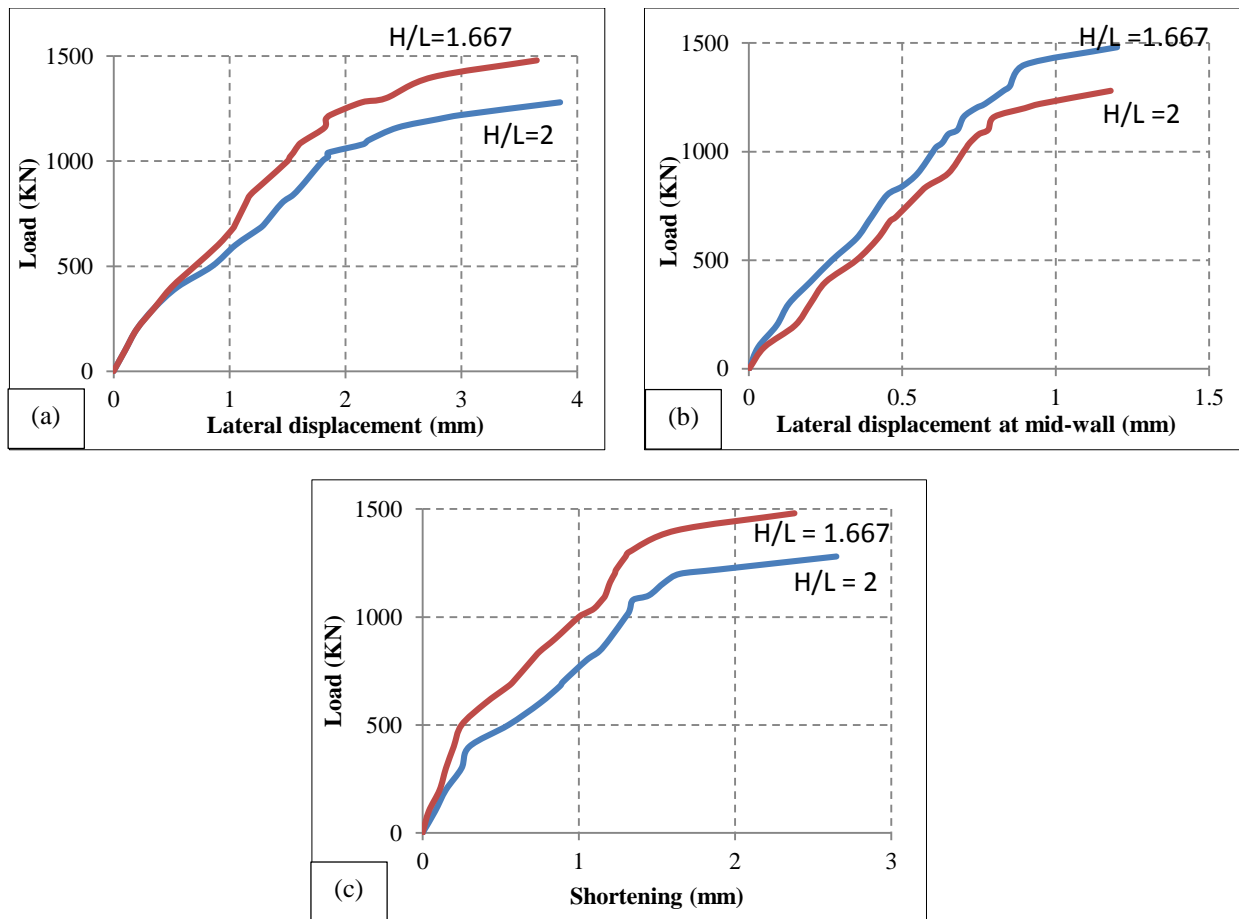
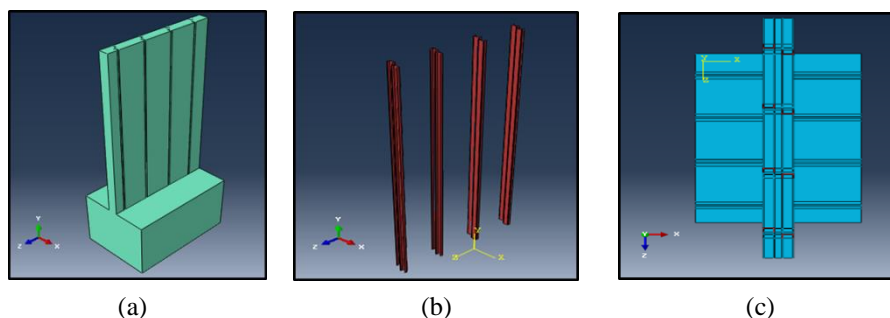
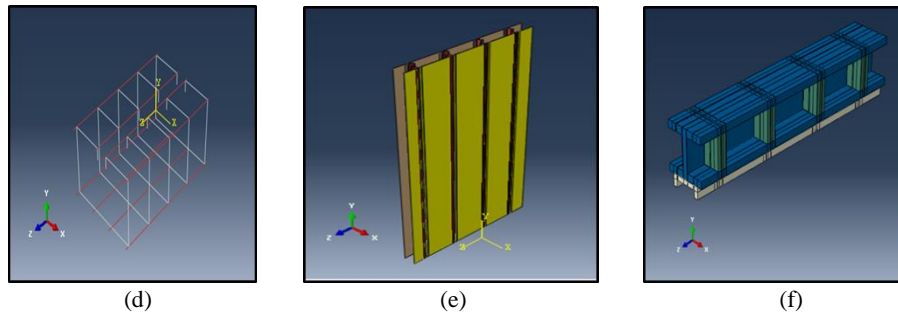


Figure 14. Axial load- lateral displacement at compressive strength equal to 63.3 MPa (a) At the top height of the wall; (b) At the mid-height of the wall

### 5. Finite Element Modeling

In the present study, nonlinear three-dimensional finite element analysis is also used to evaluate the performance of the composite wall by using ABAQUS computer Program (version 6.13). Finite element results are compared with experimental results, and the comparison showed good accuracy. Different types of elements are used to model the wall specimens. Every element is described by their characteristics such as family, degree of freedoms (DOFs), the number of nodes, integration method and formulation [21]. Three-dimensional solid element C3D8R is used to model both of concrete infill, foundation, steel frame as well as the steel channel, meanwhile linear quadrilateral four-node shell (S4R) element is used to model the two faceplates. The steel reinforcement is modeled as a one-dimensional element (wire) by solid, beam or truss element. The using of a solid element is expensive, thus not chosen. As reinforcement bars do not supply very high bending stiffness, the truss element is used and modeled as an embedded element. Embedded elements are allowed to have rotational degrees of freedom, but these rotations are not constrained by the embedding using the embedded element. The concrete damage plasticity (CDP) is adopted in this study because of its ability to represent the nonlinear properties of concrete. The stress-strain constitutive relation for both steel reinforcement and steel plates, steel channel is presented by using the elastic-perfectly plastic approach. The FE model of composite walls is generated firstly by creating the structural parts of the composite walls which are modeled by using pre-defined elements in Abaqus. See Figure 15.





**Figure 15. Modeling of (a) Concrete part; (b) Set of steel channel; (c) Wall part with a set of steel channel; (d) Set of steel reinforcement; (e) Steel plate with steel channel; (f) Steel frame**

After that, the step module contains defining the analysis steps, identifying output requests, as well as analysis controls, is created. The ‘Initial’ step is created by default and a step named ‘step1’ is produced for the general-static analysis. Time incrementation is the property of ‘step 1’ step.

Then, the finite element model of composite walls is created by assembling several parts. The part instances of the model are concrete infill, steel plate, steel channel, steel reinforcement, and steel frame. The assembled model contains independent part instances also has a global coordinate system. Each part instance is sited by translation and/or rotation within the assembly with respect to the global origin. Different types of connections such as a tie, embedded and interface elements are used to represent the contact between bodies. The general contact is used to is simulated the interaction between the steel plate and the concrete infill and the interaction between the steel channel and the concrete after determining interface properties (Normal behavior and Tangential behavior) by using “hard formulation” in the normal direction and “penalty friction formulation” in the tangential direction. The contact between the steel plate and the steel channel is represented by tie constraint, by regarding the surface of the steel plate as master surface and the surface of a channel attached to steel plate as a slave surface. Besides, a tie constraint is used to connect the bottom flange surface of the I-steel section frame to the web of a steel channel as well as it used to connect the stiffener to I-steel section as shown in Figure16. This paper presented an overview of some practical aspects of the use of composite sections in high-rise buildings. a unified and integrated approach to determine the axial-flexural capacity of complex cross-sections made of any combination of materials Using this approach, the analysis of all composite cross-sections can be performed in an integrated manner. The paper also discusses some recent trends and important considerations that should be kept in mind for an effective design of composite members (composite columns, shear walls, floors) and presents an overview of some of the practical aspects of composite concrete-steel construction in tall buildings. Then support and load are applied. Support is applied in the ‘Initial’ step with rotation /displacement boundary condition. Both rotation and translation are restrained in the x, y, and z-direction. The load is applied in ‘step 1’ which is applied as pressure load uniformly distributed on the top region of I-steel section as shown in Figure17. After that, the finite element analysis required the meshing of the model. In other words, the model is divided into small elements by choosing an element size of mesh in part instances as shown in Figure18.

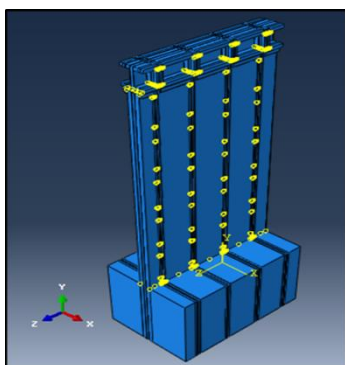


**Figure 16. Composite wall with tie constraint**

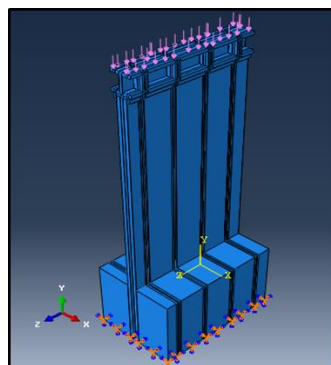


**Figure 17. the isometric view for load and boundary condition**

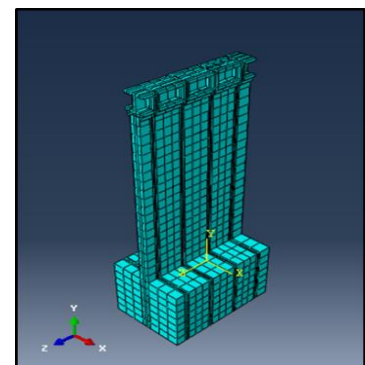


**Figure 18. Mesh formation for composite wall**

After that, the job is created which allows submitted for analysis. The results of the analysis are obtained in odb file. The results information, as well as the various model shapes such as undeformed, deformed shapes, are achieved from the output database using the visualization module. The field output requests or history outputs requests can be attained in nodal point, in elements or in the whole model based upon the specific output request. These requests can be plotted in Abaqus viewport using plotting tools, and data exported to Microsoft Excel using Excel utility option.

### 6. Validation of Composite Model

Finite element results are validated against experimental results. A finite element model was arranged by using the Abaqus computer program to verify and idealize the composite wall of the experimental work.

The deformation of the composite wall with aspect ratio 1.667 and compressive strength 39 MPa can be shown in Figure 19. In addition, Figure 20 (a) shows a comparison between numerical and experimental results of a composite wall in terms of load- lateral displacement relationship. The lateral displacement of the model is 2.7 mm which lower than experimental results by about 6.89 %. Figure 20 (b) shows that the lateral displacement at the mid-height of the model recorded a value of 0.88mm which is lower than that obtained from experimental results by about 7.36%. Figure 20 (c) illustrates that axial shortening numerically obtained by the Abaqus computer program equal to 1.75 mm which is about 7.89% lower than the value obtained experimentally.

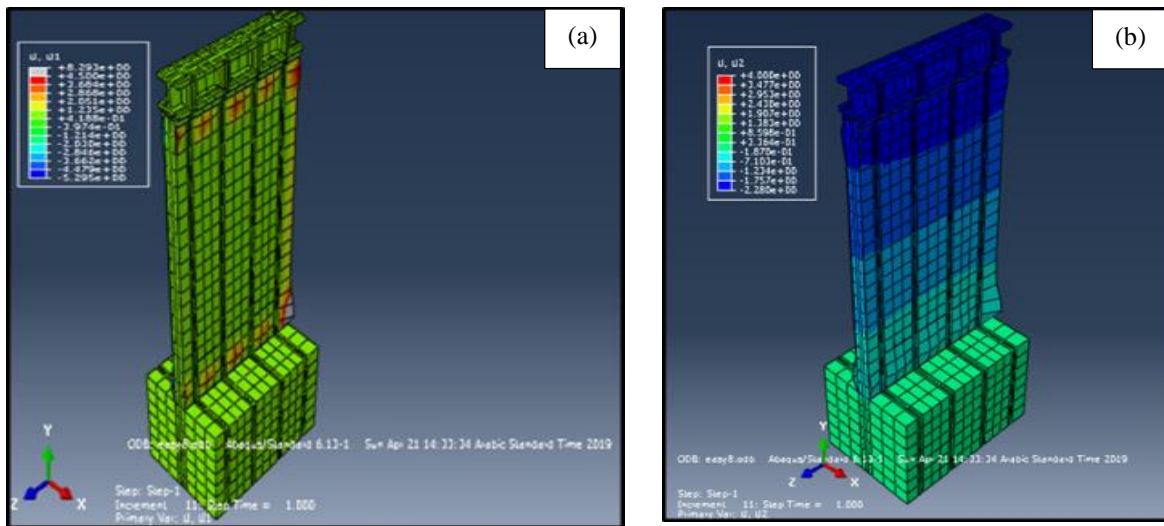


Figure 19. Deformation of composite wall in (a) X-direction (iso view); (b) Y-direction (iso view)

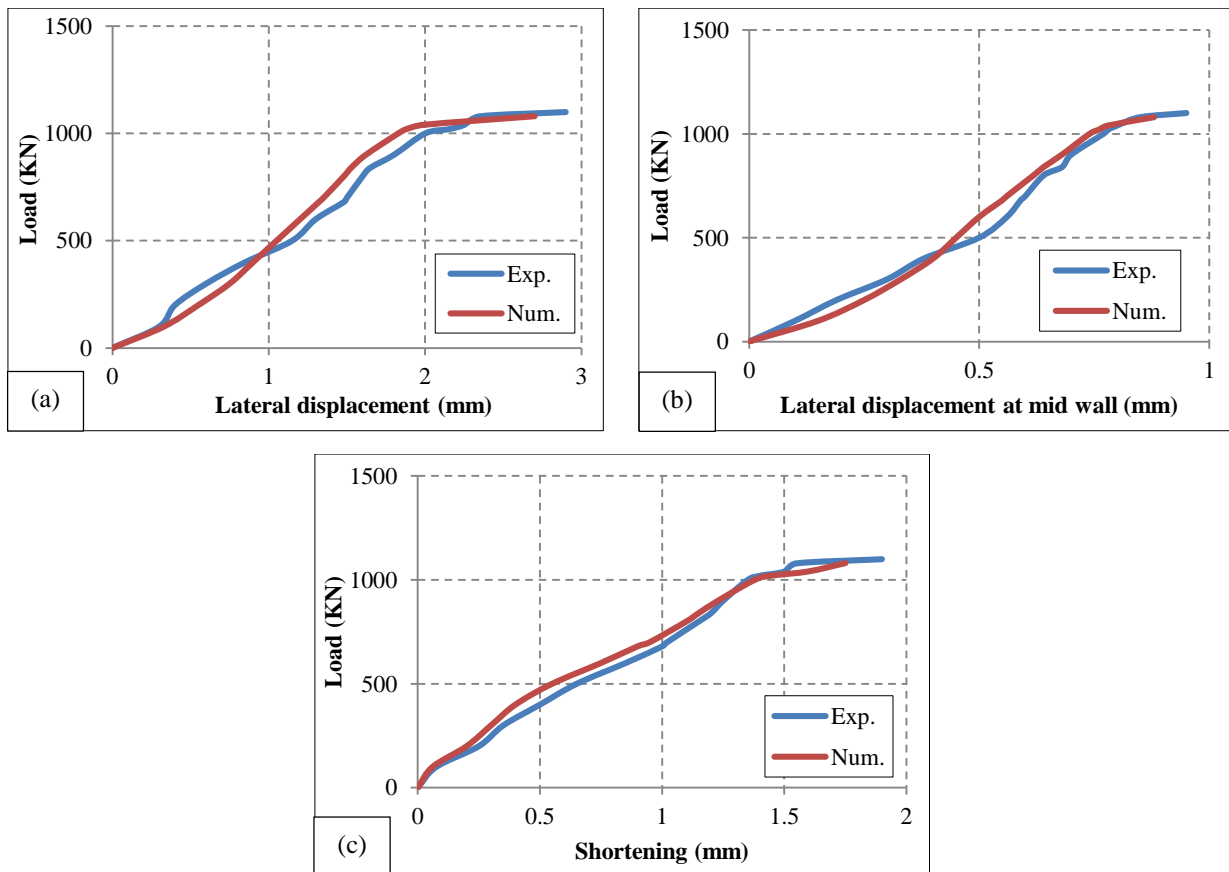


Figure 20. Results for the model with aspect ratio 1.667 and compressive strength 39 MPa (a) Load versus lateral displacement at top; (b) Load versus lateral displacement at mid-wall; (c) Load versus shortening

Figure 21 illustrates the deformation of the composite wall with aspect ratio 1.667 and compressive strength 54.75 MPa in X and Y direction. The force-displacement relationship of both the model and the composite wall can be shown in Figure 22. It can be obtained from Figure 22 (a) that the force-displacement relationship is linear until the load level 400 kN with a 5 mm deflection of the model. After that, deflection increases rapidly and has the value 3.12 mm at the failure load which is less than the lateral displacement of the wall by about 4%. The failure load for the model is 1280 kN which is 1.5% lower than the failure load for the tested wall. According to Figure 22 (b), the lateral displacement of the model equal to 0.93 mm which is lower than the experimental value by about 7%. Besides, the axial shortening of it is 2 mm which is lower than numerical results obtained from Abaqus computer program by about 9% as shown in Figure 22 (c).

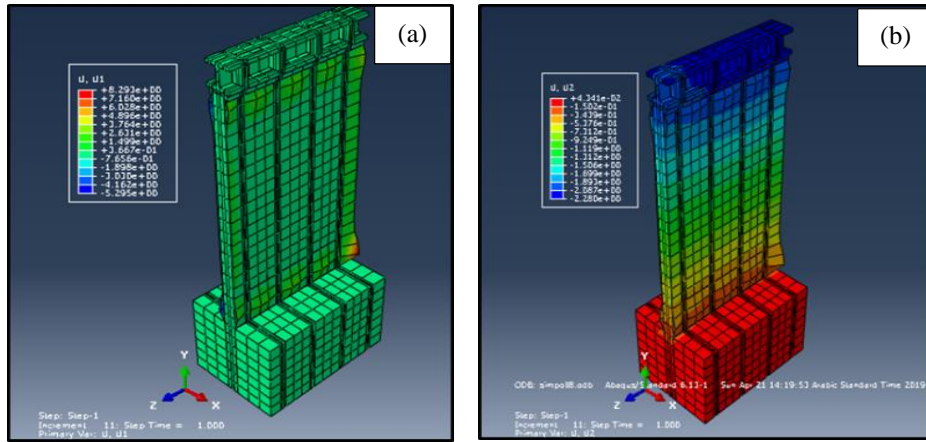


Figure 21. Deformation of composite wall in (a) X-direction (iso view); (b) Y-direction (iso view)

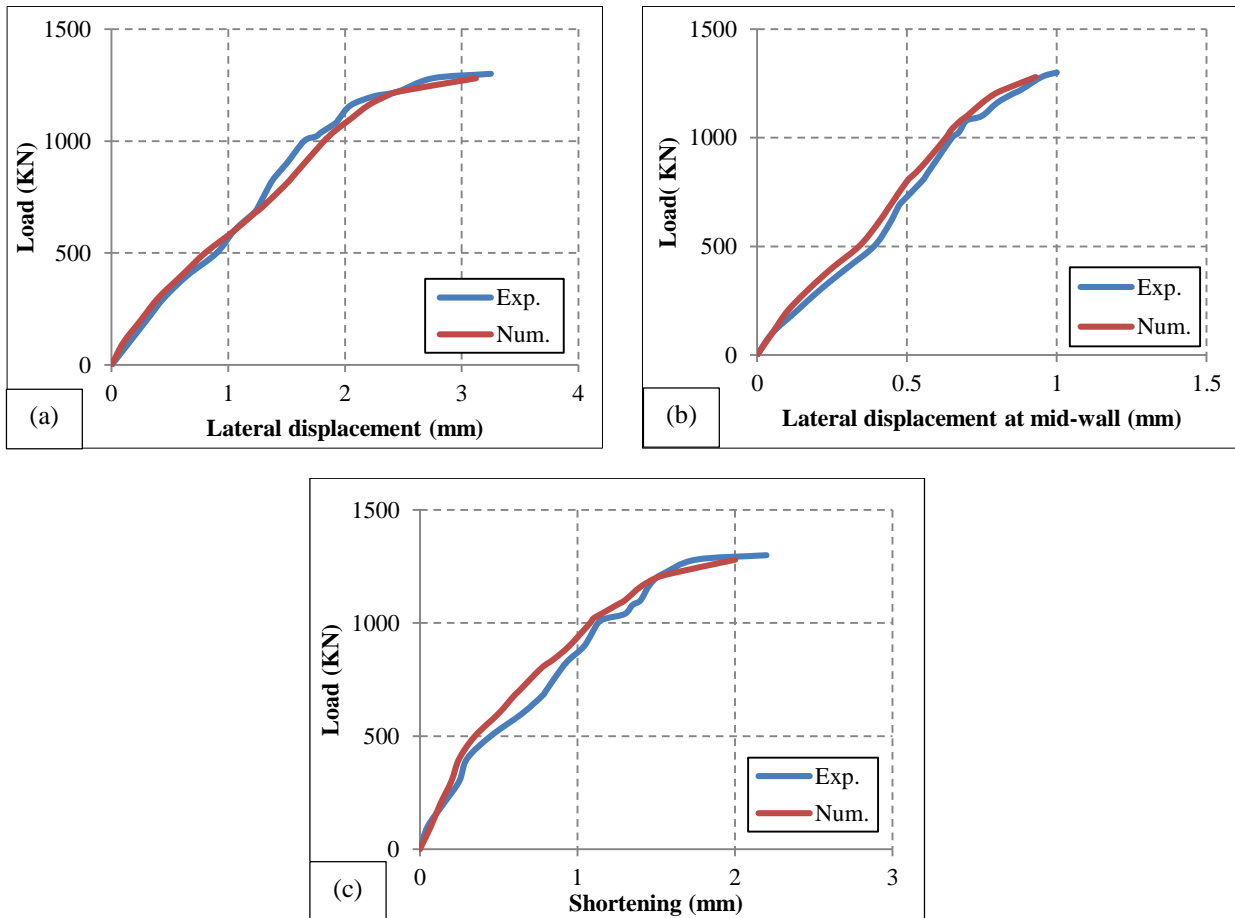


Figure 22. Results for the model with aspect ratio 1.667 and compressive strength 54.75 MPa (a) Load versus lateral displacement at top; (b) Load versus lateral displacement at mid-wall; (c) Load versus shortening

Figure 23 displays the deformation of the composite wall with aspect ratio 1.667 and compressive strength 63.3 Mpa. According to Figure 24 (a), it can be observed that the force-displacement relationship of the model and composite wall

are similar. The lateral displacement at the top height of the model was 3.5 mm at the failure load which is less than the lateral displacement of the wall by about 4.1%. The failure load for the model is 1467kN which is about 0.87% lower than the failure load for the composite wall. Also here, experimental and numerical data contains the displacement-load relationship at the mid-height of the specimen in Figure 24 (b). The model has a lateral displacement equal to 1.17 mm which is lower than the experimental value by about 2.5%. Besides, the axial shortening of it is 2.35 mm which lower than the experimental axial shortening by about 1.26% as shown in Figure 24 (c). From these figures, we can be obtained that the model is stiffer than the tested wall.

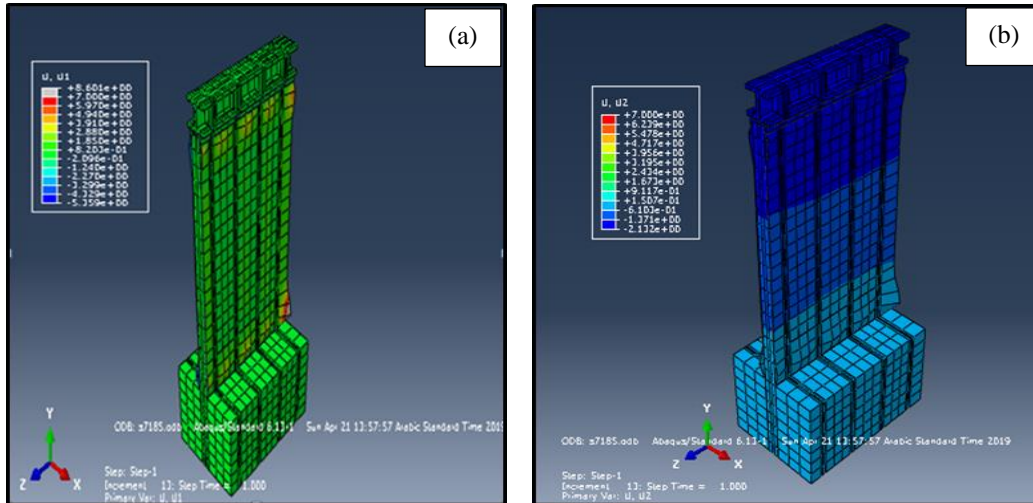


Figure 23. Deformation of composite wall in (a) X-direction (iso view) (b) Y-direction (iso view)

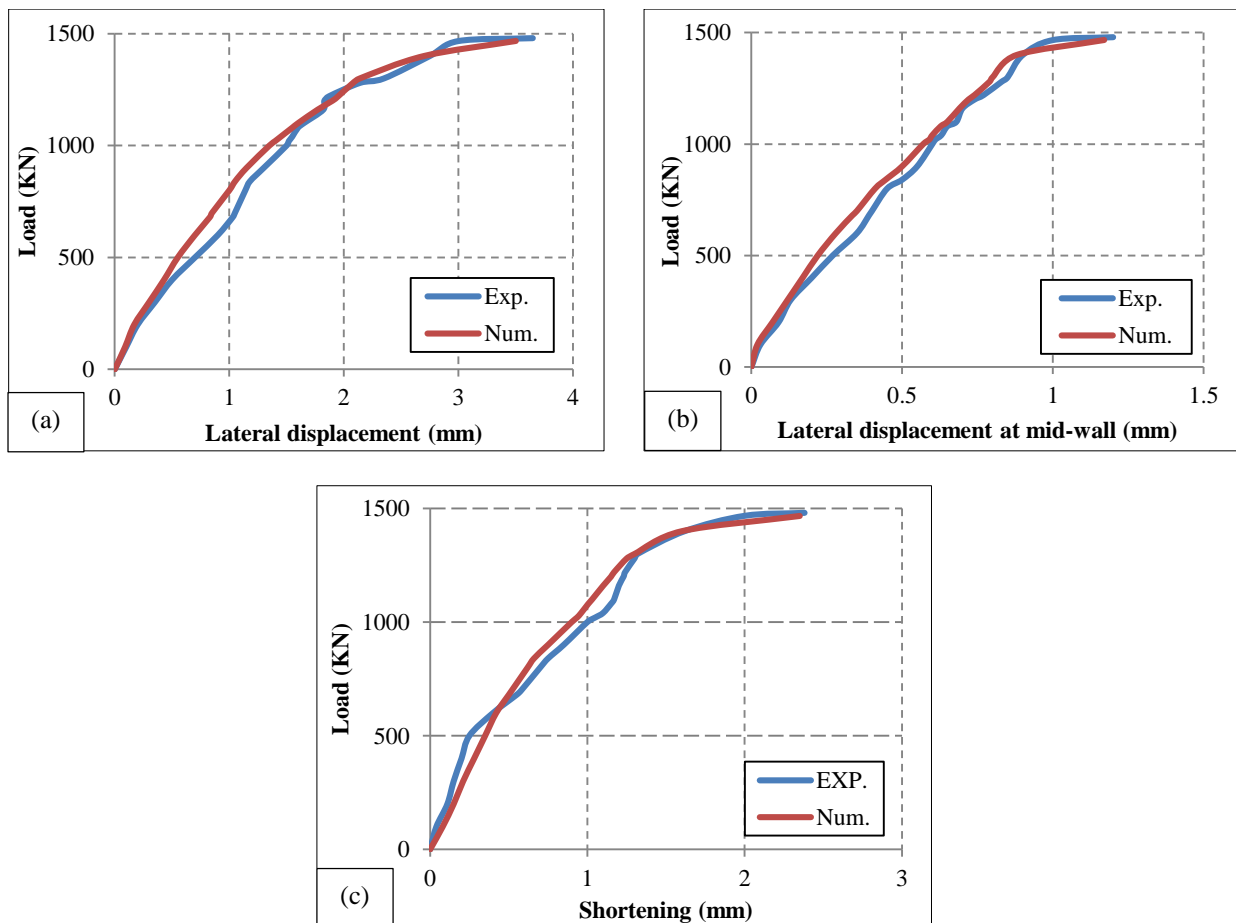


Figure 24. Results for the model with aspect ratio 1.667 and compressive strength 63.3 MPa (a) Load versus lateral displacement at top; (b) Load versus lateral displacement at mid-wall; (c) Load versus shortening

Both lateral and axial deformation of the composite wall of aspect ratio (2) and compressive strength 39 MPa can be shown in Figure 25. Besides, the force-displacement relationship of the model and the composite wall can be shown in



Figure 26 (a). The graph of the force-displacement relationship of the model seems to be linear up to 300 kN followed by increasing in lateral displacement until to reach a value of 2.8 mm lateral displacement at failure load equal 1023kN. The lateral displacement of the model is less than the lateral displacement of the wall by about 5%. The failure load for the model is lower than the failure load for the composite wall by about 1.6%. Also here, experimental and numerical data contains the displacement-load relationship at the mid-height of the wall in Figure 26 (b). The model has a lateral displacement equal to 1.08 mm which is lower than experimental value by about 3.57%. Besides, the axial shortening of it is 2.1 mm which lower than the experimental axial shortening by about 4.5% as shown in Figure 26 (c).

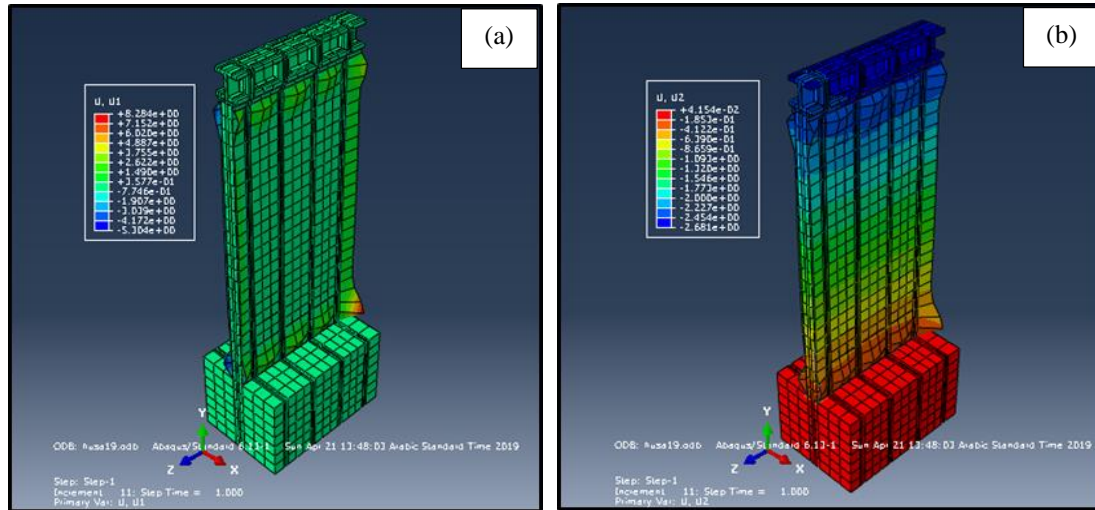


Figure 25. Deformation of composite wall in (a) X-direction (iso view); (b) Y-direction (iso view)

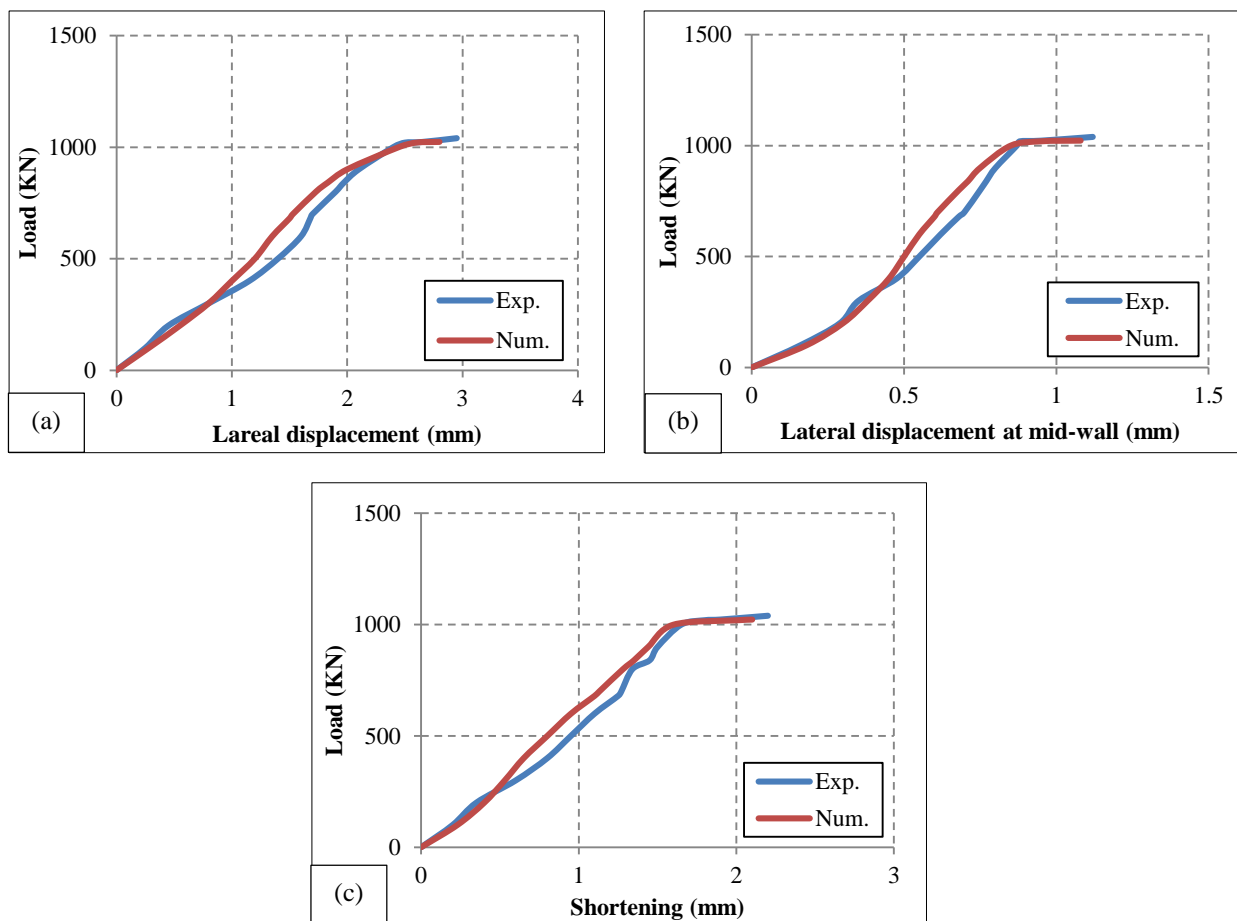


Figure 26. Results for the model with aspect ratio 2 and compressive strength 39 MPa (a) Load versus lateral displacement at top; (b) Load versus lateral displacement at mid-wall; (c) Load versus axial shortening

Figure 27 shows the lateral and axial deformation of the composite wall having aspect ratio equal to 2 and compressive strength 54.75 MPa. The results for the model are compared with those for the wall as shown in Figure 28.

Figure 28 (a) shows the load-lateral displacement relationship of the model. The lateral displacement of it at the top height of the wall is (3.25 mm) which lower than the numerical results obtained from the Abaqus computer program by about 4.4 %. The comparison of load versus displacement curve between experiment and model is shown in Figure 28 (b).The comparison shows good accuracy. The lateral displacement recorded a value of 1.12 mm which is lower than that obtained from experimental results by about 2.6%. From Figure 28 (c), it can be obtained that axial shortening numerically obtained by Abaqus computer program equal to 2.25 mm which is about 6.25 % lower than the axial force obtained experimentally.

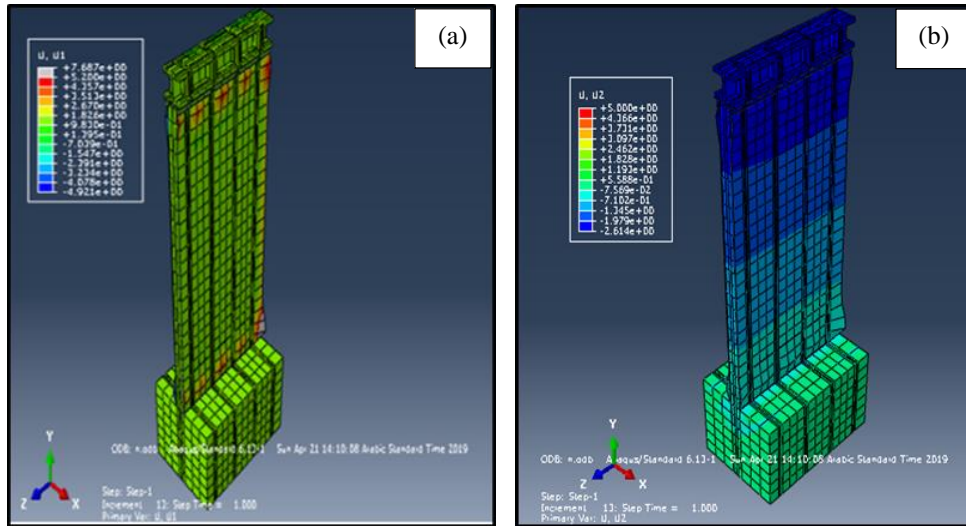


Figure 27. Deformation of composite wall in (a) X-direction (iso view); (b) Y-direction (iso view)

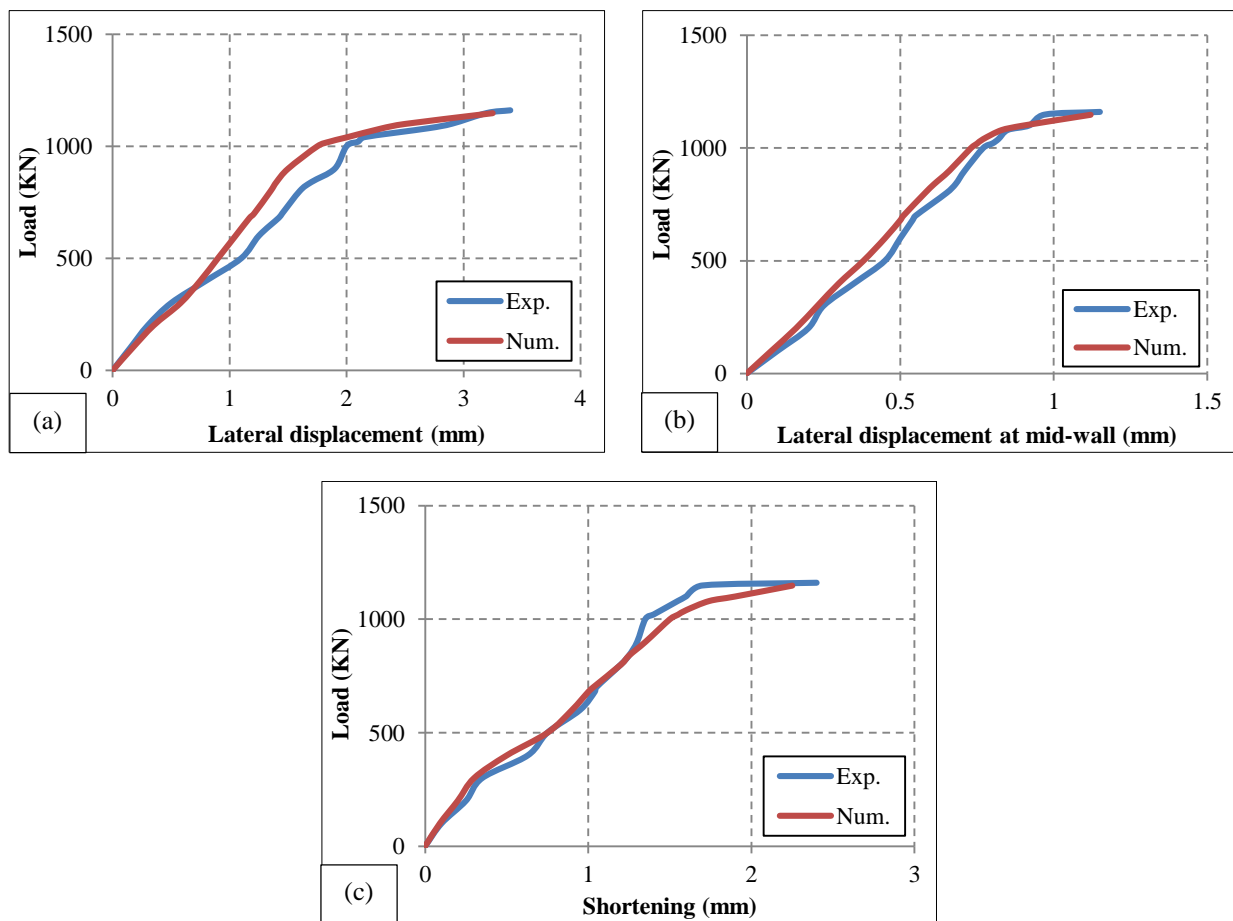


Figure 28. Results for the model with aspect ratio 2 and compressive strength 54.75 MPa (a) Load versus lateral displacement at top; (b) Load versus lateral displacement at mid-wall; (c) Load versus axial shortening

The deformation of the composite wall having aspect ratio 2 and compressive strength 63.3 MPa is shown in Figure 29. The force-displacement relationship of the model and the wall is shown in Figure 30 (a). It can be noticed that the

force-displacement relationship between the model and the wall is similar. The lateral displacement has a value of 3.65 mm at the failure load which is less than the lateral displacement of the wall by about 5.19%. The failure load for the model is 1271 kN which is 0.7% lower than the failure load for the tested wall. Also here, experimental and numerical data contains the displacement-load relationship at the mid-height of the wall in Figure 30 (b). The model has a lateral displacement equal to 1.15 mm which is lower than experimental value by about 2.5%. Besides, the axial shortening of it is 2.5 mm which lower than experimental axial shortening by about 5.66% as shown in Figure 30 (c).

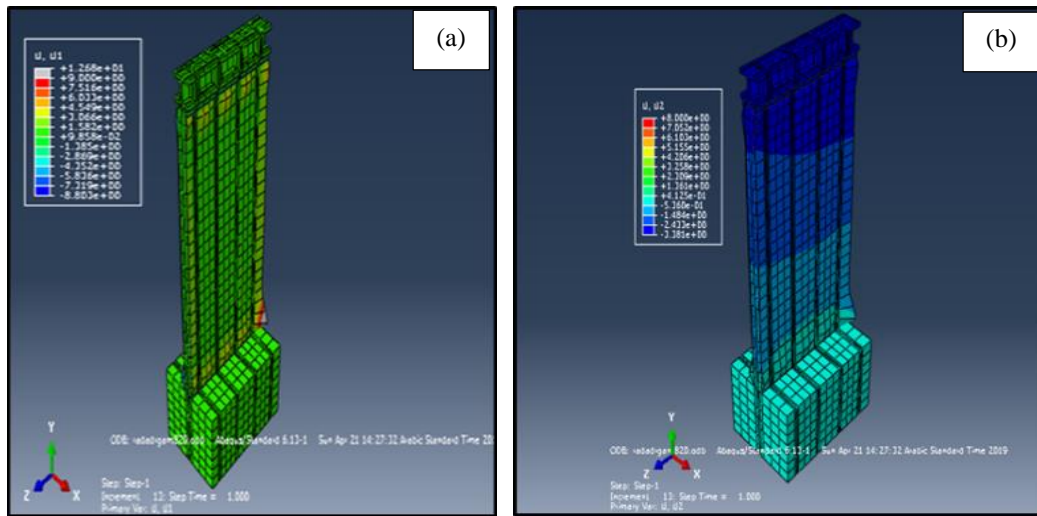


Figure 29. Deformation of composite wall in (a) X-direction (iso view); (b) Y-direction (iso view)

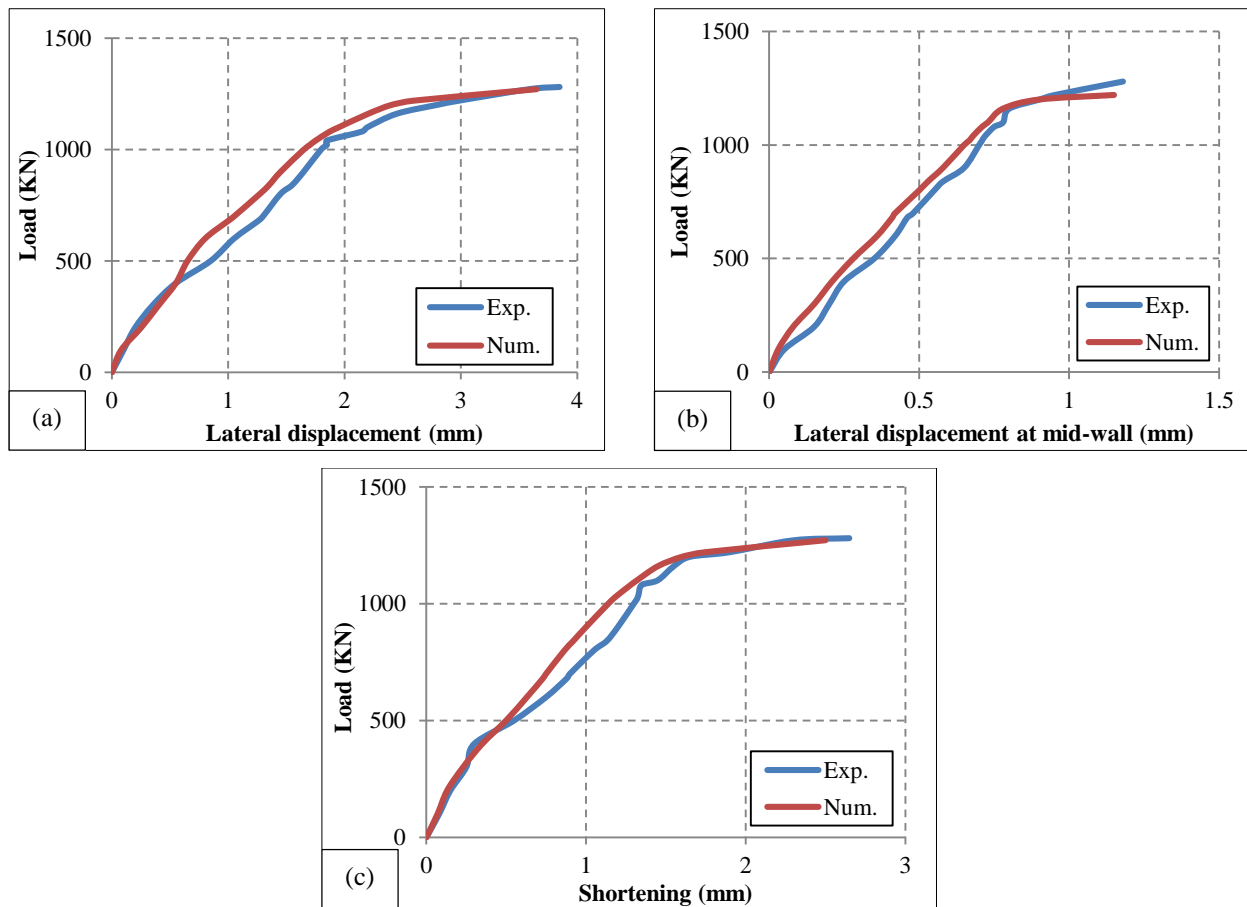


Figure 30. Results for the model with aspect ratio 2 and compressive strength 63.3 MPa (a) Load versus lateral displacement at top; (b) Load versus lateral displacement at mid-wall; (c) Load versus axial shortening

## 7. Conclusions

- Strengthening of the concrete wall by using external steel faceplates play an important role in increasing the bearing capacity of the walls and decreasing the lateral and axial displacement;
- The lateral displacement and the shortening of the composite wall depends on the strength and aspect ratio of the wall;
- As the concrete strength increased, the lateral displacement and shortening decrease at the same load;
- The lateral displacement and shortening of a composite wall with aspect ratio  $H/L=2$  is less than that of composite with low aspect ratio  $H/L=1.667$  at the same load;
- The increase in compressive strength resulted in increasing the failure load and the corresponding lateral displacement at the top and mid-height of the wall as well as the shortening of the tested wall. Accordingly, the rate of increase in failure load of the tested wall was about (34.5 %, 23.1%) as compressive strength  $f'_c$  from 39 to 63.3 (i.e. 62.3%increase) for the case of the composite wall with aspect ratio  $H/L=1.667$  and  $H/L=2$ , respectively;
- The failure load of tested walls with low aspect ratio(1.667) is more than failure load of composite walls with large aspect ratio by about (5.8, 12, 15.6%) at compressive strength (39, 54.75, 63.3 MPa), respectively and the corresponding lateral displacement at top and mid-height of the wall as well as the axial shortening are less than that having aspect ratio equal to 2 by about (1.7, 17.9, 15.8%), respectively at compressive strength 39 MPa, by about (4.6, 15, 9%), respectively at compressive strength 54.75 MPa and by about (5.5, 1.7, 11.3%), respectively at compressive strength 63.3 MPa;
- The failure mode of all the tested walls was local buckling in the left and the right side of the composite wall. The concrete infill was capable of preventing the composite wall from buckling. In all cases, failure of the composite wall was started by local buckling of the steel plate, followed by cracking and crushing of the concrete infill in the top region of the composite wall;
- The numerical results show good accuracy with experimental results.

## 8. Conflicts of Interest

The authors declare no conflict of interest.

## 9. References

- [1] Uy, B. "Strength of Short Concrete Filled High Strength Steel Box Columns." *Journal of Constructional Steel Research* 57, no. 2 (February 2001): 113–134. doi:10.1016/s0143-974x(00)00014-6.
- [2] McKinley, B, and L.F Boswell. "Behaviour of Double Skin Composite Construction." *Journal of Constructional Steel Research* 58, no. 10 (October 2002): 1347–1359. doi:10.1016/s0143-974x(02)00015-9.
- [3] Othuman Mydin, Md Azree, and Y.C. Wang. "Structural Performance of Lightweight Steel-Foamed Concrete–steel Composite Walling System Under Compression." *Thin-Walled Structures* 49, no. 1 (January 2011): 66–76. doi:10.1016/j.tws.2010.08.007.
- [4] Xiaowei, Ma, Nie Jianguo, and Tao Muxuan. "Nonlinear Finite-Element Analysis of Double-Skin Steel-Concrete Composite Shear Wall Structures." *International Journal of Engineering and Technology* (2013): 648–652. doi:10.7763/ijet.2013.v5.634.
- [5] Liew, J.Y. Richard, Jia-Bao Yan, and Zhen-Yu Huang. "Steel-Concrete-Steel Sandwich Composite Structures-Recent Innovations." *Journal of Constructional Steel Research* 130 (March 2017): 202–221. doi:10.1016/j.jcsr.2016.12.007.
- [6] Elmatzoglou, Michaela, and Aris Avdelas. "Numerical Modelling of Double-Steel Plate Composite Shear Walls." *Computation* 5, no. 4 (February 22, 2017): 12. doi:10.3390/computation5010012.
- [7] LiH, Y. "Finite Element Analysis of Local Buckling Behavior of Steel Plates in Concrete-filled Double Steel Plate Composite Shear Walls." *Journal of Building Structures* 38 (2017): 112-117. doi: 10.14006/j.jzjgxb.2017.S1.015.
- [8] Akiyama, Hiroshi, Hisashi Sekimoto, Masaaki Fukihara, Kazuo Nakanishi, and Kiyoshi Hara. "A compression and shear loading test of concrete filled steel bearing wall." In *Transactions of the 11th International Conference on Structural Mechanics in Reactor Technology* (1991).
- [9] Usami, S., H. Akiyama, M. Narikawa, K. Hara, M. Takeuchi, and N. Sasaki. "Study on a concrete filled structure for nuclear power plants (Part 2), Compressive loading tests on wall members." In *Proceedings of the 13th International Conference on Structural Mechanics in Reactor Technology (SMiRT13)*, International Association for Structural Mechanics in Reactor Technology (IASMiRT), PortoAlegre, Brazil (1995).

- [10] Choi, Byong-Jeong, Cheol-Kyu Kang, and Ho-Young Park. "Strength and Behavior of Steel Plate–concrete Wall Structures Using Ordinary and Eco-Oriented Cement Concrete under Axial Compression." *Thin-Walled Structures* 84 (November 2014): 313–324. doi:10.1016/j.tws.2014.07.008.
- [11] Zhang, Kai. "Axial compression behavior and partial composite action of SC walls in safety-related nuclear facilities." PhD diss., Purdue University, 2014.
- [12] Hao, Tingyue, Wanlin Cao, Qiyun Qiao, Yan Liu, and Wenbin Zheng. "Structural Performance of Composite Shear Walls under Compression." *Applied Sciences* 7, no. 2 (February 9, 2017): 162. doi:10.3390/app7020162.
- [13] Huang, Zhenyu, and J.Y. Richard Liew. "Compressive Resistance of Steel-Concrete-Steel Sandwich Composite Walls with J-Hook Connectors." *Journal of Constructional Steel Research* 124 (September 2016): 142–162. doi:10.1016/j.jcsr.2016.05.001.
- [14] Qin, Ying, Gan-Ping Shu, Sheng-Gang Fan, Jin-Yu Lu, Shi Cao, and Jian-Hong Han. "Strength of Double Skin Steel-Concrete Composite Walls." *International Journal of Steel Structures* 17, no. 2 (June 2017): 535–541. doi:10.1007/s13296-017-6013-9.
- [15] Eslami, Ghazaleh, and Alireza Rahai. "Experimental investigation on the behaviour of fiber reinforced light weight concrete filled double steel plate shear wall" 12th International Conference on Sandwich Structures (ICSS-12) (2018):149-151. doi:10.5075/epfl-ICSS12-2018-149-151.
- [16] Anwar, Naveed, and Fawad A. Najam. "Composite concrete-steel construction in tall buildings" 1st International Conference on Concrete and Steel Technology Engineering and Design (CASTED) (2018).
- [17] Poston, Randall W., and Charles W. Dolan. "The Framework of the 2014 American Concrete Institute (ACI) 318 Structural Concrete Building Code." *Structural Engineering International* 22, no. 2 (May 2012): 261–264. doi:10.2749/101686612x13291382990967.
- [18] ASTM C494. "Standard specification for chemical admixtures for Concrete." PA: American Society for Testing and Materials, 1999.
- [19] EFNARC, S. "Guidelines for self-compacting concrete" London, UK: Association House (2002): 32-34.
- [20] ASTM C370. "Standard specification for testing method and definitions for mechanical testing of steel products." Philadelphia, PA: American Society for Testing and Materials, 2005.
- [21] Abaqus Analysis User's Manual; Vol.1-5, SIMULA, 2009.